

# MRD-LiNet: A Novel Lightweight Hybrid CNN with Gradient-Guided Unlearning for Improved Drought Stress Identification

Aswini Kumar Patra<sup>a,b</sup>, Lingaraj Sahoo<sup>b,\*</sup>

<sup>a</sup>Department of Computer Science and Engineering, North Eastern Regional Institute of Science and Technology, Nirjuli, Itanagar, Arunachal Pradesh, 791109, India

<sup>b</sup>Department of Bioscience and Bio-Engineering, Indian Institute of Technology Guwahati, North Guwahati, Assam, 781039, India

## ARTICLE INFO

### Keywords:

Deep Learning  
Machine Unlearning  
Lightweight Convolutional Neural Network  
Drought Stress  
Precision Agriculture

## ABSTRACT

Drought stress is a major threat to global crop productivity, making its early and precise detection essential for sustainable agricultural management. Traditional approaches, though useful, are often time-consuming and labor-intensive, which has motivated the adoption of deep learning methods. In recent years, Convolutional Neural Network (CNN) and Vision Transformer architectures have been widely explored for drought stress identification; however, these models generally rely on a large number of trainable parameters, restricting their use in resource-limited and real-time agricultural settings. To address this challenge, we propose a novel lightweight hybrid CNN framework inspired by ResNet, DenseNet, and MobileNet architectures. The framework achieves a remarkable 15-fold reduction in trainable parameters compared to conventional CNN and Vision Transformer models, while maintaining competitive accuracy. In addition, we introduce a machine unlearning mechanism based on a gradient norm-based influence function, which enables targeted removal of specific training data influence, thereby improving model adaptability. The method was evaluated on an aerial image dataset of potato fields with expert-annotated healthy and drought-stressed regions. Experimental results show that our framework achieves high accuracy while substantially lowering computational costs. These findings highlight its potential as a practical, scalable, and adaptive solution for drought stress monitoring in precision agriculture, particularly under resource-constrained conditions.

## 1. Introduction

Drought stress is one of the most severe abiotic factors threatening global crop productivity and food security. Its early and precise identification is essential for timely intervention, efficient resource management, and sustaining agricultural yields [1, 2, 3]. Conventional assessment methods, including manual field inspections and physiological measurements, are often labor-intensive, subjective, and not scalable for large-scale agricultural operations. Recent advances in deep learning, particularly Convolutional Neural Networks (CNNs), have enabled automated and high-throughput analysis of plant health from aerial imagery, opening new possibilities for precision agriculture [4].

Initial research on drought and water stress relied heavily on traditional machine learning and handcrafted features. For example, Zhuang et al. [5] used color and texture features with a gradient boosting decision tree (GBDT) for water stress detection in maize, though later studies showed CNNs significantly outperformed GBDT in both accuracy and robustness [6]. Further progress has been made through advanced imaging modalities and machine learning pipelines, such as hyperspectral imaging in groundnut [7], transfer learning with DenseNet-121 for soybean drought severity [8], and hybrid CNN-LSTM approaches for chickpea [9]. Comparative studies have also reported GoogLeNet as highly accurate for multiple crops [10] and tree-based

classifiers (e.g., Random Forest, Extra Trees) as effective for chlorophyll fluorescence-based stress detection [11].

In potato crops, Butte et al. [12] applied deep learning to multi-modal aerial imagery, while Patra et al. [13] proposed an explainable CNN framework that improved classification accuracy. Other works confirmed the reliability of SVMs and Random Forests with hyperspectral data [14, 15], while Goyal et al. [16] designed a custom CNN surpassing state-of-the-art models for maize drought detection.

Recently, Vision Transformers (ViTs) have gained traction in plant stress identification due to their self-attention mechanism, which captures long-range dependencies and global context [17, 18, 19]. ViTs and hybrid variants have achieved superior performance in plant disease and stress classification [20, 21, 22, 23]. For example, ViTs have outperformed Inception V3 in tomato disease classification [24], while Perez et al. [25] demonstrated accuracy gains with a fine-tuned ViT using fewer parameters. Recent innovations include reduced transformer encoders for drought stress identification [26], lightweight modules [27], attention-head optimization [28], and transformer-CNN hybrids [29]. Despite these successes, most works emphasize accuracy, with limited focus on parameter efficiency—a key barrier for real-time deployment in resource-constrained agricultural environments.

Both advanced CNNs and ViT-based models remain computationally demanding and parameter-heavy, which limits their suitability for edge deployment and large-scale agricultural applications. To address this challenge, some recent attempts have explored lightweight models for drought stress detection, such as the approaches proposed by Patra

\*Corresponding author

✉ aswinipatra@gmail.com/akp@nerist.ac.in (A.K. Patra);

1s@iitg.ac.in (L. Sahoo)

ORCID(s):

et al. [13, 26], Li et al. [30] and Gole et al. [27]. As CNN architectures such as ResNet [31], DenseNet [32], and MobileNet [33] employ relatively fewer parameters while incorporating architectural innovations that enhance both accuracy and efficiency, their combined strengths present a promising direction. Therefore, developing a lightweight hybrid model that integrates these architectures can be highly effective and is the focus of investigation in this work.

Equally important, deployed model must adapt to evolving environmental conditions, mislabeled data, and outliers. In this context, *machine unlearning*—the process of selectively removing the influence of specific training data—has emerged as a tool for enhancing adaptability, and error correction [34, 35]. While the bulk of unlearning research focuses on privacy, there are emerging connections to plant stress detection by supporting adaptive models. Bourtoule et al. [36] proposed the foundational “Sharded, Isolated, Sliced, and Aggregated” (SISA) approach for efficient unlearning in deep models, while Cao and Yang [37] earlier formalized the notion of statistical unlearning by bounding the effect of deleted samples. Later, Ginart et al. [38] explored “amnesiac” machine learning that selectively forgets training data. Practical advances in deep neural networks include gradient-based influence estimation for fast unlearning [39], certified removal guarantees [40], and unlearning mechanisms in computer vision tasks [41]. These studies provide a strong foundation for adapting unlearning to agricultural stress identification, where mislabeled samples and environmental noise are common.

In this work, we propose a framework that addresses both efficiency and adaptability. Specifically, we:

- Design a novel lightweight hybrid CNN architecture, inspired by ResNet, DenseNet, and MobileNet, that achieves a 15-fold reduction in trainable parameters compared to CNN and ViT models, while maintaining high accuracy for drought stress identification.
- Develop a gradient norm-based machine unlearning mechanism that enables selective removal of the influence of specific training samples, thereby enhancing adaptability.
- Validate the proposed framework on a challenging real-world aerial imagery dataset of potato crops [12], demonstrating superior efficiency, performance, and scalability compared to state-of-the-art methods.

## 2. Material and Methods

### 2.1. Data Set Description

The aerial imagery of potato crops employed in this study was obtained from a publicly available, multi-modal dataset [42, 12]. The dataset was collected at the Aberdeen Research and Extension Center, University of Idaho, and is specifically designed to support machine learning research in crop health monitoring for precision agriculture. Image acquisition was performed using a Parrot Sequoia

multi-spectral camera mounted on a 3DR Solo drone. This setup provided high-resolution RGB images at  $4,608 \times 3,456$  pixels, along with four monochrome channels—green (550nm), red (660nm), red-edge (735nm), and near-infrared (790nm)—each with a resolution of  $1,280 \times 960$  pixels. The drone operated at a low altitude of 3 meters to capture detailed visual information, with a focus on identifying drought stress in Russet Burbank potato plants affected by premature senescence.

For this work, the dataset includes 360 RGB image patches in JPG format, each sized  $750 \times 750$  pixels. These patches were generated from the original high-resolution aerial images through cropping, rotation, and resizing. To expand the training data, data augmentation techniques were applied to 300 of these images following the method described by Butte et al. [12], resulting in a total of 1,500 training images. The remaining 60 images were set aside as a test set, with no augmentation applied, to ensure an unbiased evaluation of model performance.

Accurate classification required labeled data with annotated regions of interest. In this study, regions containing healthy and drought-stressed potato plants were manually annotated using the LabelImg tool [43]. Healthy plants were visually identified by their green coloration, while stressed plants appeared yellowish. Bounding boxes were drawn around these regions, and the corresponding class labels and coordinates were saved to generate ground truth annotations for model training.

In addition to RGB images, the dataset also provides corresponding spectral patches (red, green, red-edge, and near-infrared), each measuring  $416 \times 416$  pixels. However, due to the limited resolution of these monochrome images, only the RGB channels were utilized in this study.

The final augmented training set consisted of 1,500 images, while the test set comprised 60 unique images. Annotated windows (rectangular patches) were extracted from both training and test images based on the bounding box information, with each window labeled as either “healthy” or “stressed.” As depicted in Fig. 1, Fig. 1a shows an original RGB image, whereas Fig. 1b illustrates the extracted healthy and stressed regions. In the provided example, six windows correspond to healthy areas and three to stressed ones. After extraction, the final training dataset contained 11,915 stressed and 8,200 healthy image patches. The test set contains 734 stressed and 401 healthy windows extracted from the 60 test images.

## 3. Methodology

The proposed model is a novel convolutional neural network (CNN) architecture that synergistically combines the principles of **MobileNetV2**, **Resnet** and **DenseNet**. The design goal is to achieve an optimal balance between model *efficiency*, *representational power*, and *gradient flow*, critical for binary image classification tasks where both precision and computational feasibility are essential.

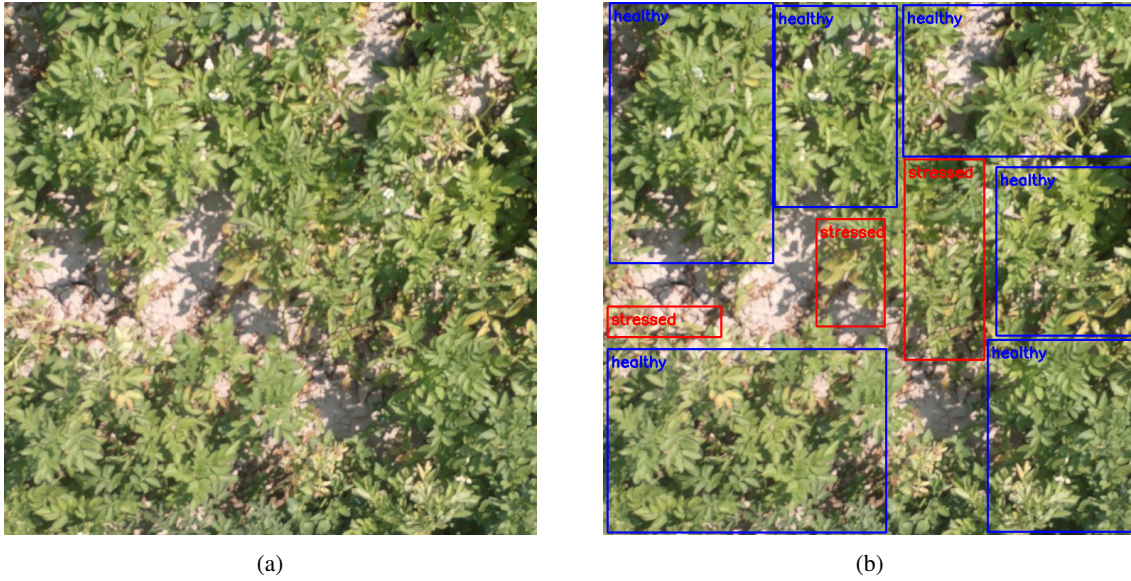


Figure 1: Field images showing a) Sample RGB image and b) Healthy and Stressed Labels.

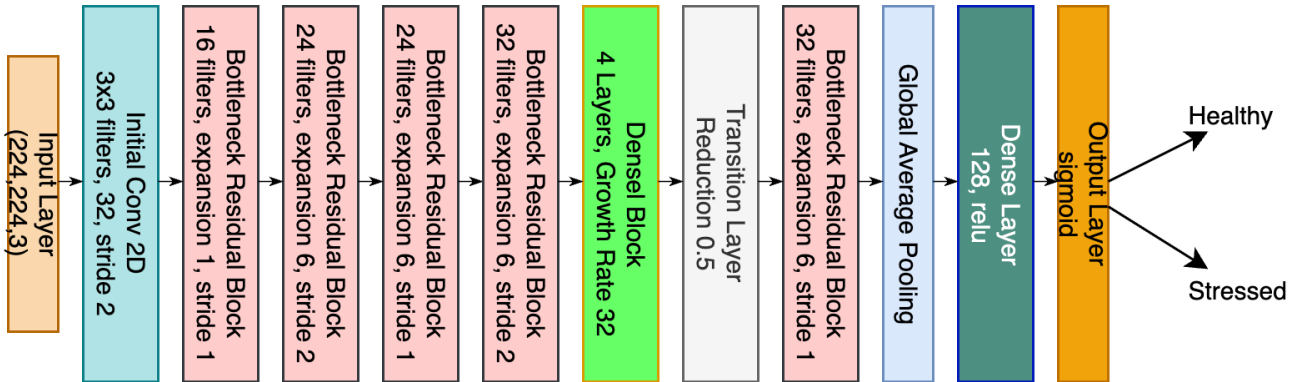


Figure 2: Schematic diagram of the lightweight network architecture

The proposed framework begins with an initial convolutional layer for low-level feature extraction, followed by four residual blocks that enable deeper feature learning through skip connections. A dense block is then employed to encourage feature reuse and efficient representation learning, after which a transition layer reduces dimensionality and controls model complexity. This is followed by a bottleneck block that captures the most salient features in a compact form. The high-level representations are aggregated using global average pooling, passed through a fully connected dense layer for further processing, and finally mapped to the output layer for prediction. The overall architecture of the proposed framework is depicted in Fig. 2, illustrating the sequence of layers from the initial convolution through to the output layer. The detailed steps and parameters of each constituent block in the proposed model are summarized in Algorithm 1. A brief description of each block follows.

### 3.0.1. Input and Initial Convolution

The model processes RGB input images with a resolution of  $224 \times 224$ . An initial convolutional layer applies 32 filters of size  $3 \times 3$  with stride 2 and “same” padding. This layer is followed by batch normalization and ReLU6 activation to standardize feature distributions and introduce non-linearity while preserving numerical stability for low-precision computation.

### 3.0.2. Bottleneck Residual Blocks

Inspired by MobileNetV2, the Bottleneck Residual Block comprises three phases:

- **Expansion Phase:** A  $1 \times 1$  pointwise convolution increases channel dimensionality, enabling a richer representation of features.
- **Depthwise Convolution:** A  $3 \times 3$  depthwise convolution performs lightweight spatial filtering independently across channels, drastically reducing computational cost.

- **Projection Phase:** A second  $1 \times 1$  convolution projects the features back to a lower dimension.

These blocks integrate *skip connections* when input and output dimensions match, preserving information and enhancing gradient flow during backpropagation. Their significance lies in reducing computation while retaining accuracy—ideal for scalable deep learning models.

### 3.0.3. Dense Block

A Dense Block consisting of four convolutional units is embedded mid-network. Each unit applies BatchNorm  $\rightarrow$  ReLU  $\rightarrow 3 \times 3$  Conv2D and concatenates its output with all preceding feature maps. This design enforces: feature reuse across layers, improved gradient propagation, diminished vanishing gradient issues, especially in deeper networks.

Dense connectivity introduces a collective memory mechanism, where each layer benefits from the cumulative knowledge of all previous layers, enhancing both convergence speed and generalization.

### 3.0.4. Transition Layer

To manage the increasing number of channels from the Dense Block, a Transition Layer is applied. It performs:

- Channel compression using a  $1 \times 1$  convolution,
- Downsampling via  $2 \times 2$  average pooling.

This module plays a *regularization role*, reducing model complexity and the risk of overfitting, while maintaining vital feature information. The transition also helps in controlling memory usage and computation.

### 3.0.5. Final Processing and Classification

Following the transition, a final Bottleneck Residual Block is applied. The feature map is then reduced to a 1D vector using Global Average Pooling (GAP), which reduces overfitting and parameter count compared to fully connected layers. A Dense Layer with 128 units and ReLU activation processes the features, followed by a sigmoid-activated output unit to generate binary classification results.

### 3.0.6. Optimization Strategy

The model is trained using the *Adam* optimizer with a scheduled exponential learning rate decay, which gradually lowers the learning rate to promote stable convergence. The initial learning rate is set to 0.001, with a decay rate of 0.9 applied every  $2 \times \text{steps\_per\_epoch}$ . Here, the steps per epoch are calculated as

$$\text{steps\_per\_epoch} = \left\lfloor \frac{\text{num\_train\_samples}}{\text{batch\_size}} \right\rfloor.$$

The **binary crossentropy** loss function is employed to handle binary classification, particularly in cases of class imbalance. The optimizer's learning rate schedule is designed to balance fast convergence at the start with fine-grained updates toward the end.

## 3.1. Machine Unlearning Mechanism

Machine unlearning refers to the concept where a model forgets or discards data used for training. This is particularly useful when certain data becomes irrelevant or when privacy issues arise (such as removing data associated with a specific individual).

In the process of machine unlearning, the model is first trained on the entire dataset. For each sample, an influence score is computed based on the gradients of the model's predictions with respect to the loss function. This score measures how much a particular sample contributed to the model's learning. The influence score for sample  $i$  can be expressed as:

$$\text{Influence Score for sample } i = \|\nabla \mathcal{L}(f(\mathbf{x}_i), y_i)\|$$

where  $\nabla \mathcal{L}$  is the gradient of the loss function  $\mathcal{L}$  with respect to the model's prediction  $f(\mathbf{x}_i)$  for sample  $i$ , and  $y_i$  is the true label.

Based on these influence scores, certain samples (such as the least influential ones) are removed from the training dataset. The rationale is that removing these samples will not significantly degrade the model's performance, but will help reduce the model's reliance on less useful or sensitive data. Formally, we can identify and discard the samples with the smallest influence scores:

$$S_{\text{remove}} = \{\mathbf{x}_i : I(\mathbf{x}_i) \text{ is among the lowest in } S\}$$

After removing the data points with the lowest influence scores, the model is retrained on the reduced dataset. This mimics a "forgetting" mechanism, as the model no longer has access to those removed data points, but retains the important features learned from the remaining data. Let  $S_{\text{new}} = S \setminus S_{\text{remove}}$  be the new training set. The model is retrained using the reduced dataset:

$$\hat{f}_{\text{new}} = \arg \min_f \sum_{\mathbf{x}_i \in S_{\text{new}}} \mathcal{L}(f(\mathbf{x}_i), y_i)$$

Thus, the model  $\hat{f}_{\text{new}}$  is updated without the influence of the removed data points, effectively forgetting them while retaining the learned features from the remaining data. Figure 3 illustrates the overall machine unlearning framework, depicting key steps from influence score calculation to data removal and model retraining.

The influence score for each image in the dataset is calculated based on the gradients of the model's predictions with respect to the input image, as explained below. The influence score indicates how much an individual image influences the model's decision. The higher the influence score, the more sensitive the model's prediction is to changes in that image.

---

**Algorithm 1:** Customized lightweight CNN Model

---

**Input:** Input shape:  $224 \times 224 \times 3$ , Training samples:  $num\_train\_samples$

**Output:** Trained CNN model with bottleneck residual blocks and DenseNet layers

**1 Sub-functions:**

- BottleneckBlock( $x$ ,  $filters$ ,  $expansion\_factor$ ,  $stride$ ):
  - Conv2D( $filters \times expansion\_factor$ , (1, 1)), BatchNorm, ReLU(6.0);
  - DepthwiseConv2D(3, 3),  $stride = stride$ , BatchNorm, ReLU(6.0);
  - Conv2D( $filters$ , (1, 1)), BatchNorm;
  - If  $stride == 1$  &  $x.shape[-1] == filters$ , skip connection;
- DenseBlock( $x$ ,  $num\_layers$ ,  $growth\_rate$ ): **for**  $i = 1$  to  $num\_layers$  **do**
  - BatchNorm, ReLU, Conv2D( $growth\_rate$ , (3, 3));
  - Concatenate input  $x$  with Conv2D output;
- TransitionLayer( $x$ ,  $reduction$ ):
  - BatchNorm, ReLU, Conv2D( $reduction \times x.shape[-1]$ , (1, 1));
  - AveragePooling (2, 2),  $strides = 2$ ;

**Main Model:**

- Input:  $224 \times 224 \times 3$ ;
- Conv2D(36, (3, 3)),  $stride = 2$ , BatchNorm, ReLU(6.0);
- BottleneckBlock( $x$ , 16, 1, 1), BottleneckBlock( $x$ , 24, 6, 2);
- BottleneckBlock( $x$ , 24, 6, 1), BottleneckBlock( $x$ , 32, 6, 2);
- DenseBlock( $x$ , 4, 32);
- TransitionLayer( $x$ , 0.5);
- BottleneckBlock( $x$ , 32, 6, 1);
- Global Average Pooling;
- Dense(128, ReLU), Dense(1, Sigmoid);
- Initial learning rate: 0.001;
- Steps per epoch:  $num\_train\_samples / batch\_size$ ;
- Exponential decay learning rate schedule;
- Compile model (Adam, Binary Crossentropy, Accuracy);

**Return:** Compiled CNN model;

---

### 3.1.1. Influence Score Calculation

To quantify how much a sample contributes to learning, we define an influence score as follows.

Given a trained model  $M$  with parameters  $\theta$ , the prediction for an input image  $\mathbf{x}$  is

$$\hat{y} = f(\mathbf{x}; \theta).$$

To quantify the effect of an image on the model's decision, we compute an *influence score* using gradients. The procedure consists of the following steps:

1. **Gradient Computation:** For each image, compute the gradient of the prediction  $\hat{y}$  with respect to the input  $\mathbf{x}$ :

$$\nabla_{\mathbf{x}} \hat{y} = \frac{\partial \hat{y}}{\partial \mathbf{x}}.$$

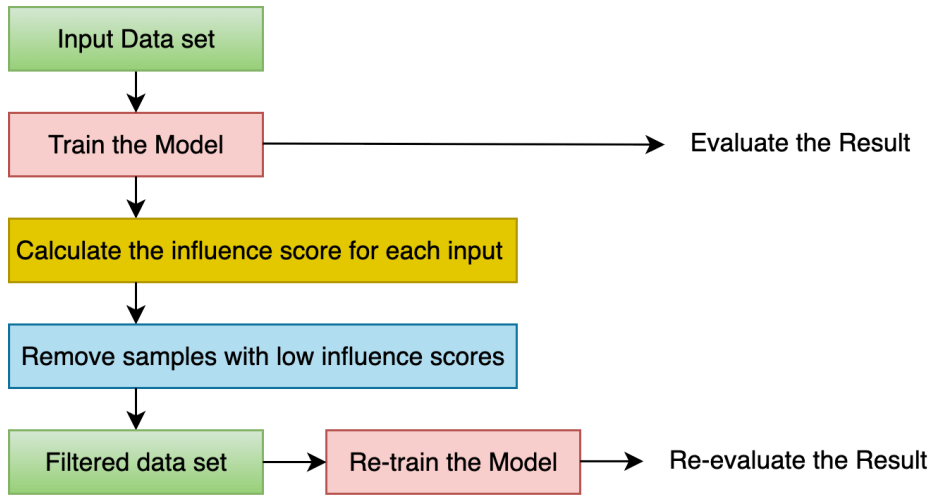


Figure 3: Machine Unlearning Framework

---

**Algorithm 2:** Calculate Influence Scores

---

**Input:** Trained model  $M$ , DataFrame  $D$  with image filenames and labels

**Output:** Array of influence scores  $S$

```

1 Initialize empty list  $S \leftarrow [ ]$ ;
2 foreach row  $r$  in  $D$  do
3    $p \leftarrow$  filename from  $r$ ;
4    $y \leftarrow$  label from  $r$  converted to float32;
5    $X \leftarrow$  PreprocessImageForCustomCNN( $p$ );
6    $G \leftarrow$  ComputeGradients( $M, X, \text{ExpandDims}(y)$ );
7   Initialize empty list  $F$ ;
8   foreach gradient tensor  $g$  in  $G$  do
9     Append Reshape( $g, (-1)$ ) to  $F$ ;
10   $V \leftarrow$  Concat( $F$ );
11   $s \leftarrow \|V\|_2$ ;
12  Append  $s$  to  $S$ ;
13 return  $S$ ;
  
```

---

This captures pixel-level sensitivity.

2. **Flattening:** Each gradient tensor is flattened into a one-dimensional vector  $\mathbf{g}$  for ease of handling.
3. **Concatenation:** Gradients from all layers,  $\mathbf{g}_1, \dots, \mathbf{g}_n$ , are concatenated into a single vector:

$$\mathbf{v} = \text{Concat}(\mathbf{g}_1, \dots, \mathbf{g}_n).$$

4. **Norm Calculation:** The L2 norm of  $\mathbf{v}$  gives the influence score:

$$s = \|\mathbf{v}\|_2 = \sqrt{\sum_i v_i^2}.$$

5. **Final Result:** Repeating the above steps for the dataset  $D$  yields an array of scores:

$$S = [s_1, s_2, \dots, s_N].$$

Algorithm 2 outlines the step-by-step procedure for computing influence scores. For each image in the dataset, the

model gradients are computed, flattened, and concatenated across layers. The L2 norm of this concatenated gradient vector yields a single scalar influence score, which quantifies the sensitivity of the model’s prediction to that image. By iterating over the dataset, the algorithm produces an array of influence scores that highlights which images exert the strongest effect on the model’s decision-making. These influence scores enable targeted data removal to facilitate efficient and effective machine unlearning.

## 4. Results and Discussion

The model was implemented in Python version 3.10.14 using machine learning libraries such as *Keras*, *TensorFlow*, *Scikit-learn*, *Pandas*, *NumPy*, and *Matplotlib*. Training was performed with a batch size of 128 for 50 epochs, optimized with the *Adam* optimizer (initial learning rate = 0.001) and *categorical cross-entropy* as the loss function.

**Table 1**  
Data Augmentation Parameters Used for Model Training

Parameter	Value
Rescale	$\frac{1}{255}$
Rotation Range	30
Width Shift Range	0.2
Height Shift Range	0.2
Shear Range	0.2
Horizontal Flip	True
Vertical Flip	True
Fill Mode	Nearest

#### 4.1. Performance of the Proposed Model

The customized CNN model was evaluated under three distinct scenarios: (i) training without augmentation, (ii) training with augmentation, and (iii) retraining with augmentation after machine unlearning (removal of 5% training data).

Eight augmentation techniques were applied to the training dataset, including rescaling, rotation, width and height shifting, shear transformation, zooming, and horizontal flipping. These parameters (Table 1) expanded data variability and helped mitigate overfitting. Their role in stabilizing training dynamics is further highlighted in the learning curve analysis (Fig. 5).

To quantify the contribution of individual training samples, influence scores were calculated as described in Section 3.1.1. The histogram of scores (Fig. 4) revealed that while most samples exerted moderate influence, a subset exhibited either very high or very low values. In the proposed unlearning strategy, the least influential 5% of samples were excluded, since their removal was expected to reduce noise and redundancy without significantly degrading model performance. This formed the basis of the machine unlearning step, aimed at reducing reliance on less useful data. The resulting reduced dataset was then used to retrain the model, effectively forgetting the discarded samples while retaining the critical patterns learned from the remaining data.

##### 4.1.1. Learning curves

The training and validation behavior of the CNN under different experimental settings is shown in Fig 5. In the no augmentation scenario (Fig. 5a), training accuracy increased rapidly and plateaued near 0.99, whereas validation accuracy fluctuated widely during the first 20 epochs before stabilizing around 0.95. The divergence between training and validation loss, along with the instability of validation loss, indicates overfitting and limited generalization despite high training accuracy.

With the introduction of data augmentation (Fig. 5b), both training and validation curves exhibited improved stability. Validation accuracy consistently tracked training accuracy above 0.90, and validation loss displayed fewer spikes compared to the no-augmentation setting. These results confirm that augmentation enhanced generalization and convergence stability.

The augmentation with machine unlearning (5%) configuration (Fig. 5c) produced the most stable training dynamics. Training and validation accuracies converged smoothly above 0.93, with both loss curves showing steady declines and minimal divergence. Importantly, validation fluctuations were further reduced compared to the augmentation-only scenario, suggesting that machine unlearning contributed to robust generalization, reduced overfitting, and improved reliability across epochs.

##### 4.1.2. Confusion Matrices and Classification Report

The quantitative evaluation results are summarized in Table 2, with confusion matrices shown in Fig. 6.

**Scenario-wise classification outcomes** In the no augmentation setting, the framework achieved an overall accuracy of 88.1%. The stressed class exhibited high precision (0.97) but comparatively lower recall (0.84), leading to misclassification of stressed samples as healthy. The confusion matrix (Fig. 6a) confirms this, with 119 stressed samples incorrectly labeled as healthy, highlighting the model’s tendency to under-detect stress conditions despite the healthy class achieving a strong recall of 0.96.

The augmentation-only scenario improved both stability and generalization. Accuracy rose slightly to 88.6%, with stressed precision maintained at 0.98 and recall remaining at 0.84. The confusion matrix (Fig. 6b) illustrates a modest reduction in misclassifications, with 115 stressed samples misclassified as healthy and only 14 false positives among healthy samples. This indicates that augmentation reduced the imbalance and improved class separability.

The augmentation with machine unlearning (Aug + MU, 5%) scenario yielded the best overall results. Accuracy peaked at 90.0%, with stressed recall improving to 0.87 and F1-score to 0.92, while the healthy class achieved precision of 0.80 and recall of 0.96. As depicted in the confusion matrix (Fig. 6c), false negatives for stressed samples decreased to 99, the lowest across all scenarios, with only 15 false positives for the healthy class. This demonstrates that machine unlearning reduced error rates, and minimized false negatives compared to the other two settings.

**Comparative insights** Taken together, the results from Table 2 and Fig. 6 highlight that stressed class predictions benefited the most from augmentation and unlearning, as recall consistently improved (0.84 → 0.87). Meanwhile, the healthy class maintained strong recall across all scenarios but exhibited notable gains in precision under the Aug + MU configuration. These improvements emphasize that the integration of data augmentation with machine unlearning achieves the best trade-off between precision and recall, yielding a more generalizable and balanced framework for classification.

#### 4.2. Comparison of Performance

The comparative performance of the proposed CNN framework against existing state-of-the-art models is summarized in Table 3. Prior pipelines such as MobileNet [13] and DenseNet121 [13] achieved respectable accuracies of 88.7% and 90.7%, respectively, while the ViT-TL model

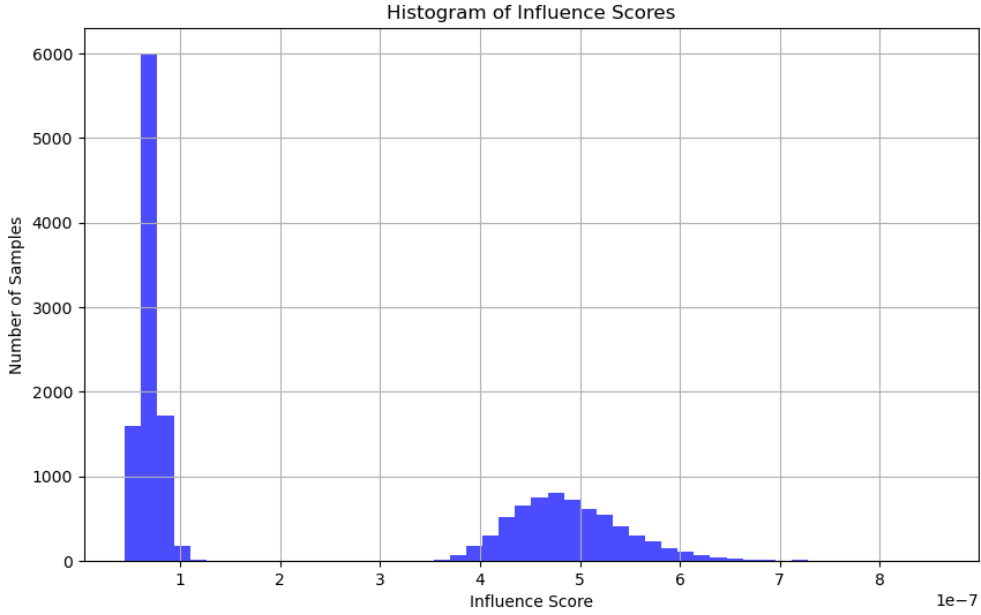


Figure 4: Distribution of influence scores for training samples (50 bins).

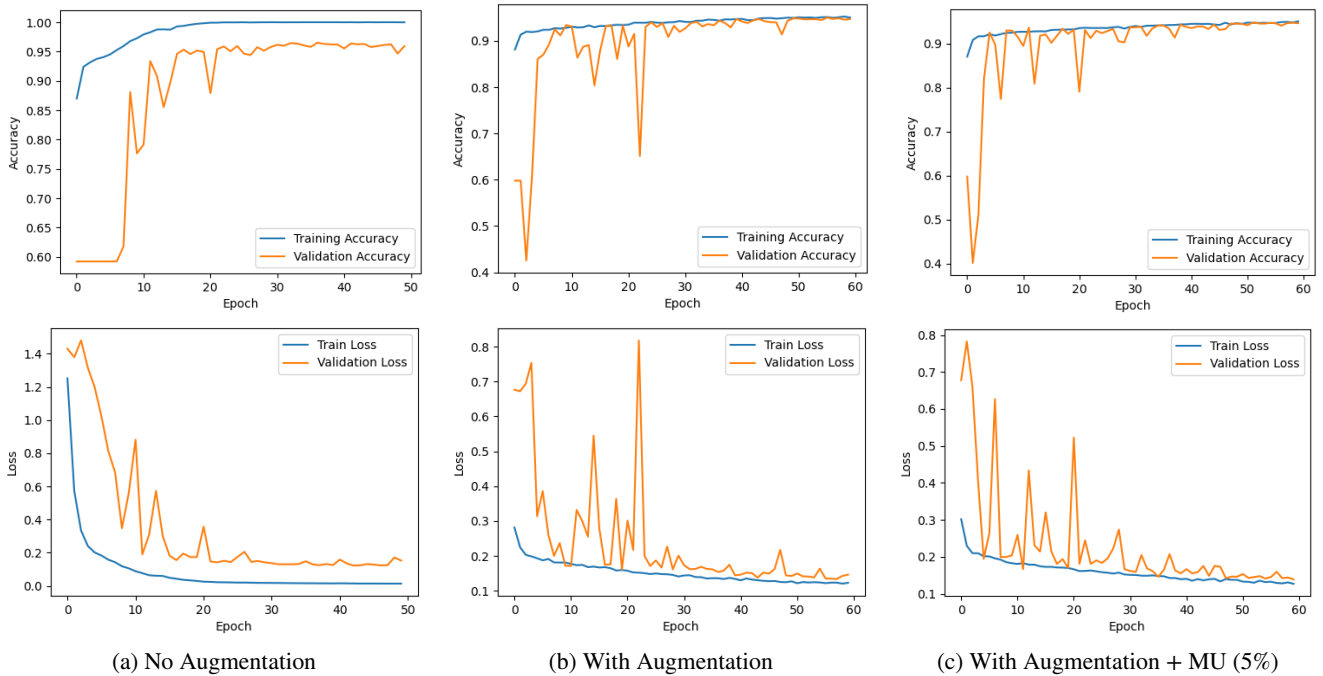


Figure 5: Learning curves (accuracy and loss) for the CNN under three scenarios: (a) without augmentation, (b) with augmentation, and (c) with augmentation + machine unlearning (5% data removal). Each subfigure shows Accuracy (top) and Loss (bottom).

[26] reached the highest reported accuracy of 91.6%. These transformer-based and deep CNN architectures, however, come with significantly larger parameter counts (ranging from 3.5M to 12M), which demand higher computational resources and longer training times.

In contrast, the proposed framework attains a competitive accuracy of 90.0% with stressed and healthy F1-scores

of 0.922 and 0.874, respectively. Notably, this is achieved with only 0.231M trainable parameters, representing a 15 to 60 fold reduction in model complexity compared to existing pipelines. The lightweight design translates to reduced memory footprint, faster inference, and improved deployability on edge devices or low-resource settings, where computational constraints often limit the use of heavier architectures.

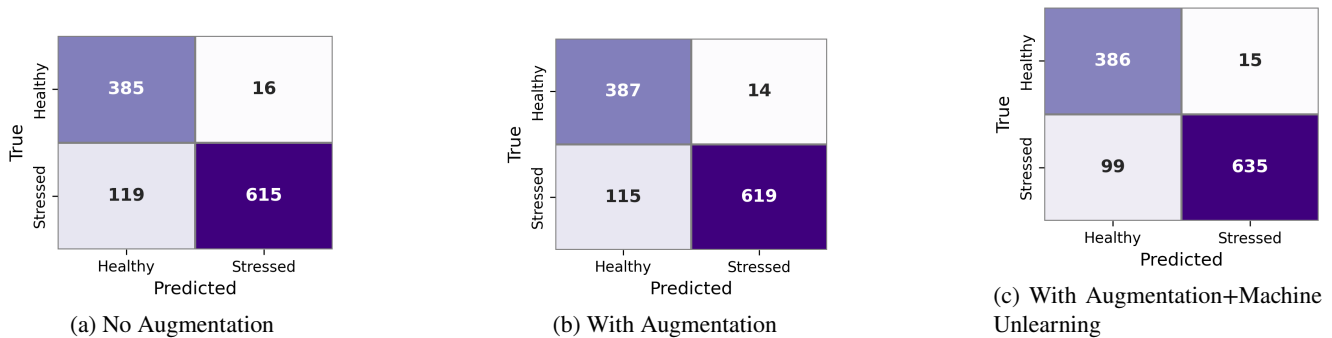


Figure 6: Confusion matrices for the three scenario.

Table 2

Comparative performance summary of the proposed framework in three scenarios. Bold values indicate the best within each column.

Scenario	Stressed			Healthy			Accuracy	Key Notes
	Precision	Recall	F1-score	Precision	Recall	F1-score		
No Augmentation	0.97	0.84	0.90	0.76	<b>0.96*</b>	0.85	0.881	Overfits, unstable validation
With Augmentation	<b>0.98*</b>	0.84	0.91	0.77	<b>0.97*</b>	0.86	0.886	Better generalization, stable curves
With Aug + MU (5%)	<b>0.98*</b>	<b>0.87</b>	<b>0.92</b>	<b>0.80</b>	0.96	<b>0.87</b>	<b>0.900</b>	Best balance, robust generalization, fewer false negatives

Another critical insight lies in class-specific performance. While MobileNet and DenseNet pipelines tend to favor healthy class recall, and ViT-TL maximizes stressed class recall, our proposed model achieves a more balanced trade-off between precision and recall across both classes. This is particularly important for stress detection tasks, where false negatives (misclassifying stressed plants as healthy) carry greater risk for agricultural monitoring and decision-making. The machine unlearning strategy further reduced such errors, resulting in the lowest stressed-class false negative rate (13.5%) among the evaluated models.

Taken together, these findings highlight that the proposed framework delivers state-of-the-art performance with minimal computational overhead, making it well-suited for real-world applications where resource efficiency and balanced predictive power are equally critical. By bridging the gap between accuracy and efficiency, the framework offers a

practical alternative to heavy-weight architectures, without compromising generalization.

## 5. Conclusion

This study proposed a lightweight hybrid CNN integrated with gradient-guided machine unlearning for drought stress identification in potato crops. The framework achieved 90.0% accuracy with only 0.231M parameters, offering state-of-the-art performance with at least 15-fold fewer parameters than existing models. Unlike heavier CNN or transformer-based pipelines, the proposed model delivered a balanced trade-off between precision and recall, while reducing false negatives in stressed plants—a critical requirement for agricultural monitoring. Its compact design makes it highly suitable for real-time deployment in UAVs, edge devices, and other resource-constrained settings. Future

Table 3

Comparative performance evaluation of various existing works

Model	Stressed		Healthy		F1-Score (Stressed)	F1-Score (Healthy)	Test Accuracy	Trainable Parameters
	Precision	Recall	Precision	Recall				
MobileNet based Pipeline [13]	0.978	0.845	0.773	0.965	0.906	0.862	0.887	3.5 Million
DenseNet121 based Pipeline [13]	0.967	0.887	0.820	0.945	0.925	0.880	0.907	7.09 Million
ViT-TL [26]	0.968	0.901	0.839	0.945	0.934	0.890	0.916	14M
Proposed Framework (Aug + MU) *	0.980	0.870	0.800	0.960	0.922	0.874	0.900	0.231M

work will emphasize expanding to multimodal imagery, improving interpretability, and validating performance across diverse crops and field conditions.

## References

- [1] Jose Luis Araus and Jill E. Cairns. Field high-throughput phenotyping: the new crop breeding frontier. *Trends in Plant Science*, 19(1):52–61, January 2014.
- [2] Ali Razaq, Parwinder Kaur, Naheed Akhter, Shabir Hussain Wani, and Fozia Saleem. Next-generation breeding strategies for climate-ready crops. *FRONTIERS IN PLANT SCIENCE*, 12, JUL 21 2021.
- [3] M. Farooq, A. Wahid, N. Kobayashi, D. Fujita, and S. M. A. Basra. Plant Drought Stress: Effects, Mechanisms and Management. In Eric Lichtfouse, Mireille Navarrete, Philippe Debaeke, Souchere Veronique, and Caroline Alberola, editors, *Sustainable Agriculture*, pages 153–188. Springer Netherlands, Dordrecht, 2009.
- [4] A. Kamilaris and F. X. Prenafeta-Boldo. A review of the use of convolutional neural networks in agriculture. *The Journal of Agricultural Science*, 156(3):312–322, April 2018.
- [5] Shuo Zhuang, Ping Wang, Boran Jiang, Maosong Li, and Zhihong Gong. Early detection of water stress in maize based on digital images. *Computers and Electronics in Agriculture*, 140:461–468, 2017.
- [6] Jiangyong An, Wanyi Li, Maosong Li, Sanrong Cui, and Huanran Yue. Identification and Classification of Maize Drought Stress Using Deep Convolutional Neural Network. *Symmetry*, 11(2):256, 2019.
- [7] Adduru U. G. Sankararao, P. Rajalakshmi, and Sunita Choudhary. Machine Learning-Based Ensemble Band Selection for Early Water Stress Identification in Groundnut Canopy Using UAV-Based Hyperspectral Imaging. *IEEE Geoscience and Remote Sensing Letters*, 20:1–5, 2023.
- [8] Paula Ramos-Giraldo, Chris Reberg-Horton, Anna M. Locke, Steven Mirsky, and Edgar Lobaton. Drought Stress Detection Using Low-Cost Computer Vision Systems and Machine Learning Techniques. *IT Professional*, 22(3):27–29, 2020.
- [9] Shiva Azimi, Rohan Wadhawan, and Tapan K. Gandhi. Intelligent monitoring of stress induced by water deficiency in plants using deep learning. *IEEE Transactions on Instrumentation and Measurement*, 70:1–13, 2021.
- [10] Narendra Singh Chandel, Subir Kumar Chakraborty, Yogesh Anand Rajwade, Kumkum Dubey, Mukesh K. Tiwari, and Dilip Jat. Identifying crop water stress using deep learning models. *Neural Computing and Applications*, 33(10):5353–5367, 2021.
- [11] Ankita Gupta, Lakhwinder Kaur, and Gurmeet Kaur. Drought stress detection technique for wheat crop using machine learning. *PeerJ Computer Science*, 9:e1268, 2023.
- [12] Sujata Butte, Vakanski, Aleksandar, Kasia Duellman, Haotian Wang, and Amin Mirkouei. Potato crop stress identification in aerial images using deep learning-based object detection. *Agronomy Journal*, 113:3991–4002, 2021.
- [13] Aswini Kumar Patra and Lingaraj Sahoo. Explainable light-weight deep learning pipeline for improved drought stress identification. *Frontiers in Plant Science*, 15:1476130, 2024.
- [14] Sizhou Chen, Jiazhi Shen, Kai Fan, Wenjun Qian, Honglian Gu, Yuchen Li, Jie Zhang, Xiao Han, Yu Wang, and Zhaotang Ding. Hyperspectral machine-learning model for screening tea germplasm resources with drought tolerance. *Frontiers in Plant Science*, 13, 2022.
- [15] Phuong D. Dao, Yuhong He, and Cameron Proctor. Plant drought impact detection using ultra-high spatial resolution hyperspectral images and machine learning. *International Journal of Applied Earth Observation and Geoinformation*, 102:102364, 2021.
- [16] Pooja Goyal, Rakesh Sharda, Mukesh Saini, and Mukesh Siag. A deep learning approach for early detection of drought stress in maize using proximal scale digital images. *Neural Computing and Applications*, 36(4):1899–1913, 2024.
- [17] Alexey Dosovitskiy, Lucas Beyer, Alexander Kolesnikov, Dirk Weissenborn, Xiaohua Zhai, Thomas Unterthiner, Mostafa Dehghani, Matthias Minderer, Georg Heigold, Sylvain Gelly, Jakob Uszkoreit, and Neil Houlsby. An image is worth 16x16 words: Transformers for image recognition at scale. <https://arxiv.org/abs/2010.11929v2>, 2021. version: 2.
- [18] Jieneng Chen, Yongyi Lu, Qihang Yu, Xiangde Luo, Ehsan Adeli, Yan Wang, Le Lu, Alan L. Yuille, and Yuyin Zhou. TransUNet: Transformers make strong encoders for medical image segmentation. <http://arxiv.org/abs/2102.04306>, 2021.
- [19] Ze Liu, Yutong Lin, Yue Cao, Han Hu, Yixuan Wei, Zheng Zhang, Stephen Lin, and Baining Guo. Swin transformer: Hierarchical vision transformer using shifted windows. <http://arxiv.org/abs/2103.14030>, 2021.
- [20] Auvick Chandra Bhowmik, Md. Taimur Ahad, Yousuf Rayhan Emon, Faruk Ahmed, Bo Song, and Yan Li. A customised vision transformer for accurate detection and classification of java plum leaf disease. *Smart Agricultural Technology*, 8:100500, 2024.
- [21] Aadarsh Kumar Singh, Akhil Rao, Pratik Chattopadhyay, Rahul Maurya, and Lokesh Singh. Effective plant disease diagnosis using vision transformer trained with leafy-generative adversarial network-generated images. *Expert Systems with Applications*, 254:124387, 2024.
- [22] Yasamin Borhani, Javad Khoramdel, and Esmail Najafi. A deep learning based approach for automated plant disease classification using vision transformer. *Scientific Reports*, 12(1):11554, 2022.
- [23] Poornima Singh Thakur, Shubhangi Chaturvedi, Pritee Khanna, Tanuja Sheorey, and Aparajita Ojha. Vision transformer meets convolutional neural network for plant disease classification. *Ecological Informatics*, 77:102245, 2023.
- [24] Utpal Barman, Parismita Sarma, Mirzanur Rahman, Vaskar Deka, Swati Lahkar, Vaishali Sharma, and Manob Jyoti Saikia. ViT-SmartAgri: Vision transformer and smartphone-based plant disease detection for smart agriculture. *Agronomy*, 14(2):327, 2024.
- [25] Sana Parez, Naqqash Dilshad, Norah Saleh Alghamdi, Turki M. Alanazi, and Jong Weon Lee. Visual intelligence in precision agriculture: Exploring plant disease detection via efficient vision transformers. *Sensors*, 23(15):6949, 2023.
- [26] Aswini Kumar Patra, Ankit Varshney, and Lingaraj Sahoo. An explainable vision transformer with transfer learning based efficient drought stress identification. *Plant Molecular Biology*, 115(4):98, 2025.
- [27] Pushkar Gole, Punam Bedi, Sudeep Marwaha, Md Ashraful Haque, and Chandan Kumar Deb. TrIncNet: a lightweight vision transformer network for identification of plant diseases. *Frontiers in Plant Science*, 14, 2023.
- [28] Huy-Tan Thai, Kim-Hung Le, and Ngan Luu-Thuy Nguyen. FormerLeaf: An efficient vision transformer for cassava leaf disease detection. *Computers and Electronics in Agriculture*, 204:107518, 2023.
- [29] Sasikala Vallabhajosyula, Venkatramaphanikumar Sistla, and Venkata Krishna Kishore Kolli. A novel hierarchical framework for plant leaf disease detection using residual vision transformer. *Heliyon*, 10(9), 2024.
- [30] Guoqiang Li, Yuchao Wang, Qing Zhao, Peiyuan Yuan, and Baofang Chang. PMVT: a lightweight vision transformer for plant disease identification on mobile devices. *Frontiers in Plant Science*, 14, 2023.
- [31] Brett Koonce. Resnet 50. In *Convolutional neural networks with swift for tensorflow: image recognition and dataset categorization*, pages 63–72. Springer, 2021.
- [32] Forrest Iandola, Matt Moskewicz, Sergey Karayev, Ross Girshick, Trevor Darrell, and Kurt Keutzer. Densenet: Implementing efficient convnet descriptor pyramids. *arXiv preprint arXiv:1404.1869*, 2014.
- [33] Andrew G Howard, Menglong Zhu, Bo Chen, Dmitry Kalenichenko, Weijun Wang, Tobias Weyand, Marco Andreetto, and Hartwig Adam. Mobilenets: Efficient convolutional neural networks for mobile vision applications. *arXiv preprint arXiv:1704.04861*, 2017.
- [34] Jie Xu, Zihan Wu, Cong Wang, and Xiaohua Jia. Machine unlearning: Solutions and challenges. *IEEE Transactions on Emerging Topics in Computational Intelligence*, 8(3):2150–2168, 2024.

- 
- [35] Chunxiao Li, Haipeng Jiang, Jiankang Chen, Yu Zhao, Shuxuan Fu, Fangming Jing, and Yu Guo. An overview of machine unlearning. *High-Confidence Computing*, 5(2):100254, 2025.
- [36] Lucas Bourtole, Varun Chandrasekaran, Christopher A Choquette-Choo, Hengrui Jia, Adelin Travers, Baiwu Zhang, David Lie, and Nicolas Papernot. Machine unlearning. In *2021 IEEE symposium on security and privacy (SP)*, pages 141–159. IEEE, 2021.
- [37] Yinzhi Cao and Junfeng Yang. Towards making systems forget with machine unlearning. In *2015 IEEE symposium on security and privacy*, pages 463–480. IEEE, 2015.
- [38] Laura Graves, Vineel Nagisetty, and Vijay Ganesh. Amnesiac machine learning. In *Proceedings of the AAAI Conference on Artificial Intelligence*, volume 35, pages 11516–11524, 2021.
- [39] Aditya Golatkar, Alessandro Achille, and Stefano Soatto. Eternal sunshine of the spotless net: Selective forgetting in deep networks. In *Proceedings of the IEEE/CVF conference on computer vision and pattern recognition*, pages 9304–9312, 2020.
- [40] Chuan Guo, Tom Goldstein, Awni Hannun, and Laurens Van Der Maaten. Certified data removal from machine learning models. *arXiv preprint arXiv:1911.03030*, 2019.
- [41] Meghdad Kurmanji, Peter Triantafillou, Jamie Hayes, and Eleni Triantafillou. Towards unbounded machine unlearning. *Advances in neural information processing systems*, 36:1957–1987, 2023.
- [42] A dataset of multispectral potato plants images, university of idaho. [https://www.idahofallshighered.org/vakanski/Multispectral\\_Images\\_Dataset.html](https://www.idahofallshighered.org/vakanski/Multispectral_Images_Dataset.html), 2021.
- [43] Tzatalin. Labelimg. <https://github.com/tzatalin/labelImg>, 2019.